Sensors & Transducers, Vol. 170, Issue 5, May 2014, pp. 60-66

www.sensorsportal.com

Sensors & Transducers

http://www.sensorsportal.com

Application and Research of Ultrasonic Horn in Ultrasonic Ranging System

Ju Xiaotao, Gu Lichen, Dong Xinyuan
School of Mechanical and Electronic Engineering, Xi'an University of Architecture and Technology, Xi'an Shaanxi, 710055, China
Tel.: 86-59-8220 2528, fax: 86-59-8220 2528
E-mail: juxiaotao2008@126.com

Received: 27 February 2014 /Accepted: 30 April 2014 /Published: 31 May 2014

Abstract: Aiming at the problem that echo signal is hard to recognize caused by ultrasonic energy's overquick dispersion and attenuation, a kind of ultrasonic horn is designed. According to the acoustic theory analysis, the ultrasonic horn can increase its radiation energy by improving impedance matching. The ultrasonic horn can make the directivity of sound source sharper and energy more centralized because of the large outlet. The simulation calculation and experiment results prove the effectiveness of ultrasonic horn to improve the scope of ultrasonic ranging. *Copyright © 2014 IFSA Publishing, S. L.*

Keywords: Ultrasonic horn, Impedance match, Directivity, Ultrasonic ranging.

1. Introduction

With the speeding up of urbanization process, the layout density of tower crane becomes higher in construction site. The collision accidents of tower crane frequently occur causing serious casualties and economic losses. Existing tower crane anticollision system in China and overseas can limit the rotation range of tower crane arm according to pre-classified work areas and prohibited areas, thus preventing collision accidents from happening [1]. This kind of anti-collision system lacks perception of surroundings and has many deficiencies in practical application. The work areas and prohibited areas in construction site often change into each other with the situation. The operator of tower crane needs to reset the areas requiring much time and effort. It will reduce the working efficiency of tower crane. For the deficiencies of existing products, a kind of active obstacle detection technology is urgently needed for tower crane anti-collision system.

As a kind of non-contact detection method, the ultrasonic ranging technology is widely used in robot obstacle avoidance, car radar and other fields. Compared with infrared technology and radar technology, it has such advantages as low cost, high reliability and adapting to severe environment [2]. Its basic principle is realized by measuring the time interval Δt between ultrasonic transmitted pulses and ultrasonic echoes. The distance between the obstacle and the sensor is given by

$$d = \frac{1}{2} c \cdot \Delta t \tag{1}$$

According to the comprehensive analysis on tower crane rotating speed, rotational inertia and reactional ability of the operator, there is practical significance when the warning range of the tower crane anti-collision is in 20~30 m [3]. During ultrasonic ranging over a long distance, the ultrasonic echo signal is very weak and SNR (Signal to Noise

Article number P_2033

Ratio) is low because of air attenuation and energy dispersion. This will lead to nearer detection distance (generally less than 10 m) of the ultrasonic ranging system, failing to meet the requirement of warning measurement of tower crane anti-collision. For handling the problem of energy dispersion and overquick attenuation of the ultrasonic sensor, a kind of ultrasonic horn was designed to enhance the ultrasonic radiation efficiency and improve the acoustic field directivity.

2. Effect on Radiation Energy

The ultrasonic propagation rule follows the general acoustic wave equation, which can be expressed as

$$\frac{\partial^2 p}{\partial x^2}+\left(\frac{\partial Ins}{\partial x}\right)\frac{\partial p}{\partial x}=\frac{1}{c_0^2}\frac{\partial^2 p}{\partial t^2}, \tag{2}$$

where p is the acoustic pressure, which is identical to $p(x)e^{j\omega t}$; c_0 is the acoustic velocity. The general solution of Formula (1) can be written as

$$p(x)=A(x)e^{\pm jkx} \tag{3}$$

The ultrasonic horn was seen as a kind of finite-length tube with continuously variable section. Given that sectional area of ultrasonic horn is the function of the coordinate x. The wave front of ultrasonic radiation changes in accordance with the sectional area which can be expressed as $S=S(x)$. This paper takes the exponential-type ultrasonic horn for example. The variation rule of the sectional area is expressed as

$$S(x)=S_0e^{\delta x}, \tag{4}$$

where S_0 is the inlet area of ultrasonic horn, δ is the meandering coefficient which stands for changing rate of the sectional area. r stands for sectional radius in a certain position along X-axis as shown in Fig. 1.

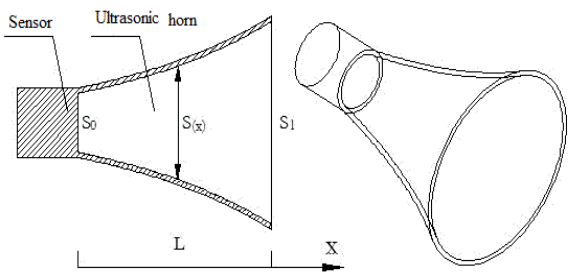

Fig. 1. Ultrasonic horn schematic diagram.

$$\pi\cdot r^2(x)=S_0e^{\delta x} \tag{5}$$

Therefore, r can be written as

$$r(x)=\sqrt{\frac{S_0}{\pi}}e^{\frac{\delta}{2}x} \tag{6}$$

The general solution of (1) may be shown that

$$p=Ae^{\frac{-\delta}{2}x+j\left(\omega t-\sqrt{k^2-\frac{\delta^2}{4}}x\right)}+Be^{\frac{-\delta}{2}x+j\left(\omega t+\sqrt{k^2-\frac{\delta^2}{4}}x\right)}, \tag{7}$$

where wave number k is identical to ω/c_0, A and B are two constant coefficients. A stands for progressive wave propagating in the positive direction, B stands for reflected wave propagating in the opposite direction.

According to the particle velocity equation,

$$v=-\frac{1}{\rho_0}\int\frac{\partial p}{\partial x}dt \tag{8}$$

The acoustic impedance of the ultrasonic horn may be shown that

$$Z_a(x)=\frac{p}{vS}=R_a(x)+jX_a(x) \tag{9}$$

$$Z_a(x)=\frac{\rho_0c_0}{S}\sqrt{1-\left(\frac{\delta^2}{2k}\right)^2}+j\frac{\rho_0c_0^2\delta}{2S\omega} \tag{10}$$

The real part $R_a(0)$ shows that the acoustic source has radiation loss when the ultrasonic sensor radiates to the ultrasonic horn inlet. Under the ideal medium study, the average loss power of ultrasonic propagation may be shown that

$$\overline{W}=\frac{1}{2}\left(R_a(0)S_0^2\right)u_a^2, \tag{11}$$

$$\overline{W}=\frac{1}{2}\rho_0c_0S_0\sqrt{1-\left(\frac{\delta c_0}{2\omega}\right)^2}u_a^2, \tag{12}$$

where u_a is the amplitude of acoustic source speed. The greater the loss power is, the more sound energy the acoustic source transports to ultrasonic horn, the farther the ultrasound spreads out. The ultrasonic source was studied in this paper. The frequency of source f is much greater than f_c, where f_c is the cutoff frequency, which is identical to $\frac{\delta c_0}{4\pi}$.

$$\overline{W} = \frac{1}{2}\rho_0 c_0 S_0 u_a^2 \tag{13}$$

If the ultrasonic horn wasn't added in front of ultrasonic sensor, the ultrasonic sensor directly radiated into the infinite air field. The radiation impedance was replaced by the impedance of infinite baffle, then

$$\overline{W} = \frac{1}{4}\rho_0 c_0 S_0 (ka_0)^2 u_a^2, \tag{14}$$

where ka_0 is much smaller than 0.5. By comparing (5) with (6), it can be shown that the power loss without ultrasonic horn is much smaller than the power loss with ultrasonic horn. Good impedance matching for the ultrasonic sensor was achieved at the outlet of the ultrasonic horn, thus increasing radiation energy of the ultrasound and helpful for ultrasonic long-distance ranging.

3. Effect on Radiation Directivity

The transducer can be treated as a plane circular piston in order to analyze its radiation characteristics. The pressure field at a distance from the transducer may be modeled using the radiating plane piston model. We can calculate the far-field sound pressure at a point $\{r,\theta\}$ due to a vibrating circular piston, as shown in Fig. 2.

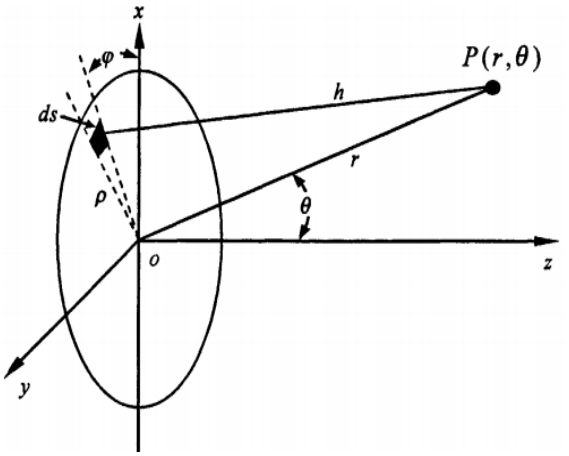

Fig. 2. The radiating plane piston model.

θ is the azimuthal angle measured with respect to radiation cone axis. The point $\{r,\theta\}$ is at radius r from the center of the transducer. The point $\{r,\theta\}$ is constrained, without loss of generality, to lie in the x-z plane. The dark region on the transducer surface denotes an infinitesimal strip, whose center point is a distance r' from the point $\{r,\theta\}$. The infinitesimal strip lies parallel to y axis, and the end of it submits an angle φ to the z axis.

The pressure at the point $\{r,\theta\}$ is calculated by considering the influence of each part of the transducer surface in turn. For computational convenience this is done by dividing the face of the piston into infinitesimal strips, themselves composed of infinitesimal simple baffled sources as defined by

$$P_z(r,t) = j\rho_0 c \frac{Qk_w}{2\pi r} e^{j\cdot(\omega t - k_w r)} \tag{15}$$

The components of this equation are listed below. j denotes the imaginary number $\sqrt{-1}$. ρ_0 is the volume density of the material (1.21 kg·m^{-3} for air). c is the speed of sound in the medium in m·s^{-1}. Q is the source strength, which is the volume of fluid displaced by the sound source per second, measured in $m^3 \cdot s^{-1}$. k_w is the inverse wavelength in rad·m^{-1}. ω is the frequency of the sound in rad·s^{-1}. t is the time, in seconds. f is the frequency of the sound wave in Hz.

Each such strip source is centered on the z axis, and has an infinitesimal source strength of

$$dQ = 2U_0 a \sin(\phi) dz, \tag{16}$$

where U_0 is the speed amplitude of the vibrating surface in m·s^{-1}, a is the radius of the transducer, ϕ is the angle between the infinitesimal element and z axis, and dz is the height of the infinitesimal strip, as shown in Fig. 2. The incremental pressure from each such infinitesimal strip source can be found by substituting the infinitesimal source strength (16) into the equation for simple baffled source (15):

$$dP_z = j\rho_0 c \frac{U_0 k_w a \sin(\phi)}{\pi r'} e^{j\cdot(\omega t - k_w r')}, \tag{17}$$

where r' is the distance from the point $\{r,\theta\}$ to each infinitesimal element making up the strip. For points $\{r,\theta\}$ in the far field, defined by $r > a^2/\lambda$. Kinsler [4] gives the approximate form

$$r' \approx r + \Delta r = r\left(1 - \frac{a}{r}\sin\theta\cos\phi\right) \tag{18}$$

Integrating the contributions from each of the infinitesimal strips (17) to form the entire contribution to the pressure field at a distant point $\{r,\theta\}$ yields

$$P_z(r,\theta,t) = j\rho_0 c\frac{U_0}{\pi r}k_w a e^{j\cdot(\omega t-k_w r)} * \int_{-a}^{a} e^{jk_w a\sin\theta\cos\phi}\sin\phi dz \tag{19}$$

This has been simplified by applying the far field approximation $r' \approx r$ in the spreading loss term, but retaining r' containing the phase information in the exponential.

Changing the variable of integration to eliminate the vertical component, z, using the relationships $z = \cos\phi$ and $dz = -a\sin\phi d\phi$, yields

$$P_z(r,\theta,t) = j\rho_0 c\frac{U_0}{\pi r}k_w a^2 e^{j\cdot(\omega t-k_w r)} * \int_{0}^{\pi} e^{jk_w a\sin\theta\cos\phi}\sin^2\phi d\phi \tag{20}$$

The minus sign has been canceled by a reversal of the range of integration. At this point it is convenient to write $k_w a\sin\theta = b$. The integral part of (20), requires special treatment, so it is defined separately

$$P_z(r,\theta,t) = j\rho_0 c\frac{U_0}{\pi r}k_w a^2 e^{j\cdot(\omega t-k_w r)} * P_z(\theta) \tag{21}$$

$$P_z(\theta) = \int_0^{\pi} e^{jb\cos\phi}\sin^2\phi\, d\phi \tag{22}$$

Turing first to the imaginary part of (22),

$$\mathrm{Im}\{p_z(\theta)\} = j\int_0^{\pi} \sin(b\cos\phi)\sin^2\phi\, d\phi \tag{23}$$

We split the range of integration in half to give

$$\mathrm{Im}\{p_z(\theta)\} = j\int_0^{\frac{\pi}{2}}\sin^2\phi\cdot\sin(b\cos\phi)d\phi + j\int_{\frac{\pi}{2}}^{\pi}\sin^2\phi\cdot\sin(b\cos\phi)d\phi \tag{24}$$

Now, changing variables $\phi = \pi - \phi'$ in the second integral yields

$$\mathrm{Im}\{p_z(\theta)\} = j\int_0^{\frac{\pi}{2}}\sin^2\phi\cdot\sin(b\cos\phi)d\phi - j\int_{\frac{\pi}{2}}^{0}\sin^2\phi'\cdot\sin(-b\cos\phi')d\phi' \tag{25}$$

Taking the negation out of the sin function and reversing the range of integration yields

$$\mathrm{Im}\{p_z(\theta)\} = j\int_0^{\frac{\pi}{2}}\sin^2\phi\cdot\sin(b\cos\phi)d\phi - j\int_0^{\frac{\pi}{2}}\sin^2\phi'\cdot\sin(-b\cos\phi')d\phi' \tag{26}$$

This forms the difference between two equal terms, and is equal to zero. Thus the imaginary part of the exponential integral (22) is also zero.

Turning now to the real part of (22), integral tables show that

$$\mathrm{Re}\{p_z(\theta)\} = \int_0^{\pi}\cos(b\cos\phi)\sin^2\phi\, d\phi, \tag{27}$$

$$\mathrm{Re}\{p_z(\theta)\} = \frac{\pi J_1(b)}{b}, \tag{28}$$

where $J_1(x)$ is the Bessel function of the first kind. Equation (28) does not evaluate formally at $b = 0$, but evaluating the limit of equation (28) as yields the value as the result. Substituting $b = k_w a\sin\theta$ again, the final equation for the complex pressure, $P_z(r,\theta,t)$, in the far field is

(if $0 < |\theta| \le \frac{\pi}{2}$)

$$P_z(r,\theta,t) = j\rho_0 c\frac{U_0}{r}k_w a^2 e^{j(\omega t-k_w r)} * [\frac{2J_1(k_w a\sin\theta)}{k_w a\sin\theta}] \tag{29}$$

(if $\theta = 0$)

$$P_z(r,\theta,t) = j\rho_0 c\frac{U_0}{r}k_w a^2 e^{j(\omega t-k_w r)} \tag{30}$$

$$\mathrm{D}(\theta) = \frac{P_z(r,\theta,t)_\theta}{P_z(r,\theta,t)_{\theta=0}} = \frac{2J_1(k_w a\sin\theta)}{k_w a\sin\theta} \tag{31}$$

The term in brackets is known as the directivity function as it gives the variation of pressure with direction [5]. Larger values of $D(\theta)$ indicate that the beam energy is concentrated into a smaller area. Smaller values of $D(\theta)$ indicate that the beam energy is spread over a larger area. The equation shows that the shape of the beam changes with frequency and radius of the ultrasonic transducer. The beam angle is wide at low frequencies, while the beam angle is narrow at high frequencies. Therefore the ultrasonic radiation scope is larger at low frequencies than at high frequencies. Furthermore, large ultrasonic transducers have higher directivity than small transducers. In other words, the larger the outlet area of ultrasonic horn is, the more concentrated the beam energy is. The smaller the outlet area of ultrasonic horn is, the more dispersive the beam energy is.

Because the outlet of ultrasonic horn is bigger than the ultrasonic transducers, the directivity of ultrasonic horn is higher than the ultrasonic transducers. So the ultrasonic horn can improve the scope of ultrasonic ranging. The ultrasonic field

directivity was simulated using Matlab software. Polar directivity diagram of ultrasonic horn was shown in Fig. 3, Fig. 4 and Fig. 5 for several different outlet areas.

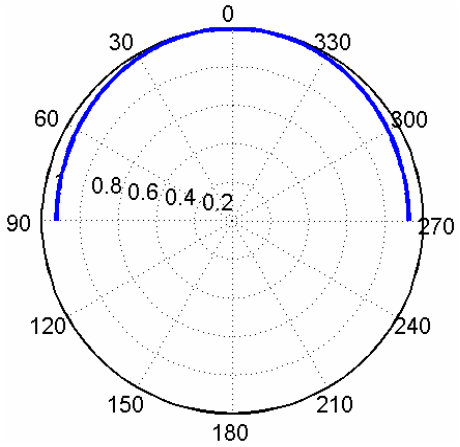

Fig. 3. Polar directivity diagram for ultrasonic horn with $ka = \pi / 5$.

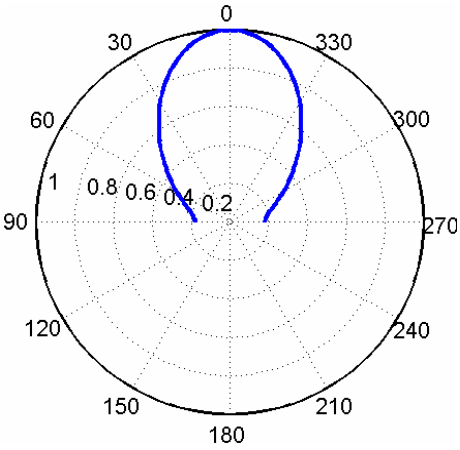

Fig. 4. Polar directivity diagram for ultrasonic horn with $ka = \pi$.

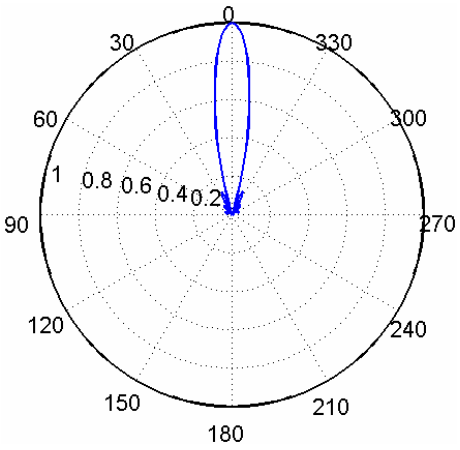

Fig. 5. Polar directivity diagram for ultrasonic horn with $ka = 4\pi$.

From Fig. 3, it can be seen that the ultrasonic directivity is increasingly high and energy is increasingly concentrated while the outlet radius of ultrasonic horn becoming constantly large. The opening area of the designed ultrasonic horn is much larger than the radiation area of ultrasonic sensor, which is beneficial to implement long-distance ultrasonic ranging.

4. Experiment

The switch power supply module was supplied for the long-distance ultrasonic ranging system. The output voltage was 300 V. Ultrasonic impulses were transmitted by the single chip microcomputer. These ultrasonic impulses were amplified as high voltage impulses by ultrasonic transmitting circuit. Then they stimulate ultrasonic transducer to transmit the ultrasound. It returns after encountering obstacles. The amplified ultrasonic echoes were sampled by the virtual instrument [6]. The time of flight (TOF) is measured by ranging algorithm, thus calculating the distance between the sensor and the obstacle. The block diagram of long-distance ultrasonic ranging system is shown in Fig. 6.

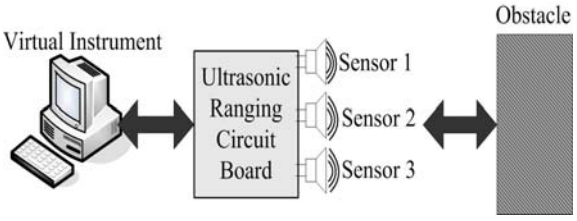

Fig. 6. Block diagram of long-distance ultrasonic ranging system.

When choosing the ultrasonic sensor, the performance parameters such as operating frequency, directivity, operating voltage should be considered. The ultrasonic sensor used in experiments is piezoelectric ceramics waterproofing ultrasonic sensor. It is widely used in ranging occasions in which the medium is air. Its main performance parameters are shown in Table 1.

The ultrasonic ranging experimental system of tower crane is shown in Fig. 5.

The dimensions of the obstacle are 120.0 cm (Width) × 84.5 cm (Height) × 2.2 cm (Thickness). The experiments are implemented at ambient temperature 29 °C. Table 2 presents the experimental results of cross-correlation method.

The experiment was implemented at the distance of 6 m away from the obstacles. The validation was conducted by comparing the echo amplitude from the transducer with horn with the one from the transducer without horn. Fig. 7 is the ultrasonic echo of the obstacles at the distance of 6m away from the

sensor without the ultrasonic horn as the ultrasonic echo was magnified 20 times. Fig. 8 is the ultrasonic echo of the obstacles at the distance of 6 m away from the sensor with the ultrasonic horn as the ultrasonic echo was magnified 20 times.

The ultrasonic wave is restrained by the transducer with the horn, which can make the ultrasonic energy centralized and the voltage echo amplitude increased obviously. From the Table 2, the horn is beneficial to improve the ultrasonic radiation efficiency and increase the distance of ranging. ▲ means that ultrasonic ranging system can't detect obstacles.

Table 1. Parameters of ultrasonic sensor.

Type	LHQ22-2
Operating frequency (**kHz**)	22.0±1
Beam angle (°)	14±2 (-3 dB)
Operating voltage (**V**)	<4000

Table 2. Experiment result.

Actual distance (m)	**Measured value with horn (m)**	**Measured value without horn (m)**
2.00	2.00	2.01
4.00	4.03	4.06
6.00	6.05	6.08
8.00	8.09	8.11
10.00	10.10	10.15
12.00	12.16	12.15
14.00	14.17	14.20
16.00	16.22	16.22
18.00	18.24	▲
20.00	20.24	▲
22.00	22.33	▲
24.00	24.33	▲
26.00	26.33	▲
28.00	28.37	▲
30.00	30.41	▲

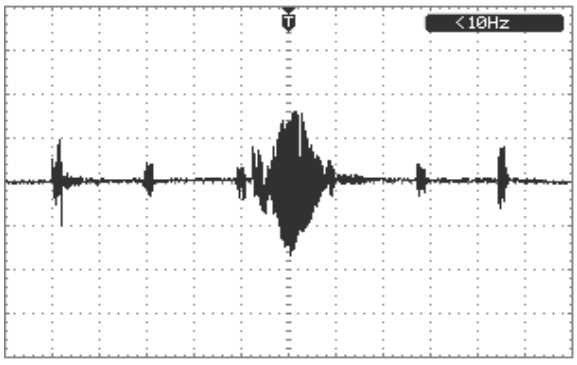

Fig. 7. Echo waveform of the sensor without the horn at the distance of 6 m away from the obstacles.

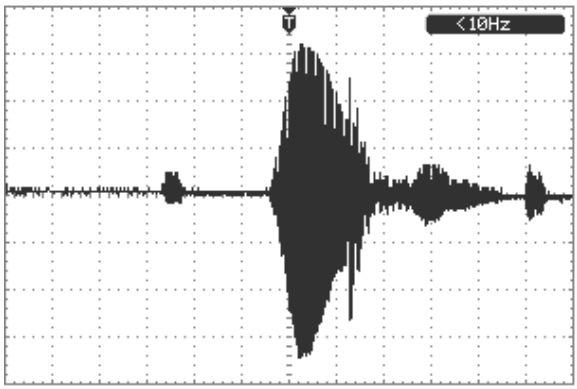

Fig. 8. Echo waveform of the sensor with the horn at the distance of 6 m away from the obstacles.

5. Conclusions

The acoustic radiation efficiency of ultrasonic horn is low and sound attenuation is large in practical application, thus affecting the detection range. Adding the ultrasonic horn is to change the bonded area size between the outlet of ultrasonic sensor and infinite air field and improve the acoustic directivity and sound field distribution, this makes acoustic radiation energy focused and ultrasonic propagating farther. Apart from that, the ultrasonic horn matches the appropriate acoustic impedance for sound source, increasing the sound power by a large margin and improving the ultrasonic propagating efficiency. As a result, the application of obstacle avoidance in long-distance ranging can be achieved. Furthermore, the effect of sound source frequency on sound attenuation should be noticed. This paper studies the effects of the radiation efficiency of sound field, energy distribution and directivity on ultrasonic propagation distance from the perspective of theoretical analysis, analog computation and experimental verification, demonstrating the feasibility of ultrasonic horn in long-distance ranging.

Acknowledgements

The authors gratefully acknowledge support from the National Natural Science Foundation of China under Grant No. 50975218 and Science Foundation of Shan Xi province under Grant No. 2013JK1011.

References

[1]. Tower cranes anti-collision, boundary and zone protection system on http://www.tac3000.com.

[2]. B. Barshan, Fast Processing Techniques for Accurate Ultrasonic Range Measurements, *Measurement*, 11, 2000, pp. 45-50.

[3]. Yan Xiaole, Gu Lichen, Time-delay estimation of ultrasonic echoes based on the physical model matching, in *Proceedings of the 8th IEEE International Conference on Automation Science and Engineering*, Seoul, Korea, August 2012, pp. 469-473.
[4]. Kinsler L. E., et al., Fundamentals of Acoustics, 3rd ed., *John Wiley and Sons,* New York, 1982.
[5]. D. K. Ksu, F. J. Margetan, D. O. Thompson, Bessel beam ultrasonic transducer: fabrication method and experimental results, *Appl. Phys. Lett*, 55, 1989, pp. 2066-2068.
[6]. Ju Xiaotao, Gu Lichen, Long distance ultrasonic ranging system oriented to tower crane anti collision, in *Proceedings of the 2nd International Conference on Machine Design and Manufacturing Engineering*, 366, 2013, pp. 609-612.